International Communications in Heat and Mass Transfer 142 (2023) 106622

Contents lists available at ScienceDirect

International Communications in Heat and Mass Transfer

journal homepage: www.elsevier.com/locate/ichmt

# Vapor condensation induced by fast-moving liquid film in the presence of noncondensable gas molecules

Kotaro Ohashi, Kazumichi Kobayashi *, Hiroyuki Fujii, Masao Watanabe

*Division of Mechanical and Space Engineering, Faculty of Engineering, Hokkaido University, Kita 13 Nishi 8, Kita-ku, Sapporo 060-8628, Hokkaido, Japan*

ARTICLE INFO

*Keywords:*
Kinetic boundary condition
Evaporation and condensation coefficients
Enskog–Vlasov equation
Kinetic theory
Noncondensable gas
Cavitation-bubble collapse

ABSTRACT

In this study, vapor condensation phenomena at the surface of a fast-moving planar liquid film in a gas mixture (vapor and noncondensable (NC) gas), aimed to imitate a cavitation bubble collapse, were simulated to investigate the evaporation and condensation coefficients of vapor molecules based on the Enskog–Vlasov equation. These coefficients indicate the evaporation and condensation rates of vapor molecules, and they were incorporated into the kinetic boundary condition (KBC) for the vapor/gas–liquid interface. We employed the Enskog–Vlasov direct simulation Monte Carlo method to simulate the condensation phenomena. Based on the results, we confirmed that the obtained coefficients decreased with an increase in the liquid temperature and NC gas content at the condensing interface. Additionally, the coefficients had the same values as those in the equilibrium state, even for such a moving system. Notably, the nonequilibrium effect on condensation phenomenon discussed in the field of cavitation bubble dynamics, whereby vapor molecules fail to condense when the liquid velocity is significantly high, could not be confirmed in this simulation. Furthermore, we conducted an analysis based on the Boltzmann equation using the direct simulation Monte Carlo method to verify the obtained coefficients.

## 1. Introduction

Heat and mass transfer induced by evaporation and condensation at the surface of a fast-moving liquid are important phenomena for cavitation-bubble collapse. Cavitation-bubble collapse has been discussed for many years; further, it has been demonstrated that vapor condensation is an essential factor influencing the maximum pressure and temperature of the internal gas during bubble collapse [1–4]. When a bubble collapses, the velocity of the vapor–liquid interface can easily exceed the speed of sound of the gas. Fujikawa and Akamatsu [1] reported that, when the velocity of the interface is sufficiently high, the vapor molecules fail to condense into a liquid because they do not have sufficient time for condensation. This is termed as nonequilibrium effect on condensation.

Conversely, a recent study on bubble dynamics analyzed the collapse phenomena of bubbles containing a gas mixture consisting of a vapor and a noncondensable (NC) gas [5]. The results suggested that the condensation of vapor molecules is suppressed by the residence of the NC gas at the vapor–liquid interface under extreme bubble-collapse conditions. In this case, the suppression of vapor-molecule condensation caused by the presence of the NC gas molecules is molecular-scale phenomenon that requires molecular-scale analyses.

To treat vapor flows with evaporation and condensation phenomena, molecular gas dynamics [6] are applicable to nonequilibrium flow analyses using the Boltzmann equation with a kinetic boundary condition (KBC) at the vapor/gas–liquid interface. Here, the KBC is the boundary condition at the vapor–liquid interface for the Boltzmann equation. The KBC entails two key parameters: the evaporation and condensation coefficients. These coefficients indicate the evaporation and condensation rates at the interface [7]. Many researchers have used molecular simulations to determine the coefficient values for mostly pure vapor molecules [8–17]. These results indicate that the evaporation and condensation coefficients have values close to unity under low liquid temperatures. Furthermore, evaporation and condensation of pure water vapor, assuming a fast-moving liquid, has also been studied using molecular dynamics (MD) [17]. In the MD simulation, the liquid film is not actually moving at high speed, but rather simulates a high-speed liquid by increasing the relative molecular velocity toward the gas. This study shows that the evaporation and condensation coefficients of pure vapor take values close to unity even when the liquid is moving at

* Corresponding author.
*E-mail address:* kobakazu@eng.hokudai.ac.jp (K. Kobayashi).

https://doi.org/10.1016/j.icheatmasstransfer.2023.106622

high speed. However, these coefficients must be small to represent the nonequilibrium effect on condensation during bubble collapse; for instance, the values are $O(10^{-2})$ in [1,2]. Therefore, significant differences exist between the molecular simulation results and bubble dynamics analyses in terms of the knowledge of these coefficients.

Recently, certain researchers determined the coefficients of vapor molecules in the presence of NC gas molecules under equilibrium states [18,19], and weak nonequilibrium states using the two-surface problem [20], and the net evaporation problem [21] based on molecular simulations. The values decreased with an increase in the NC gas molecule content at the interface and the liquid temperature, aligned tendency with experimental results [22]. Additionally, the coefficients in the weak nonequilibrium state featured the same values as those in the equilibrium state. However, it still remains unclear whether these coefficients can be applied to various nonequilibrium conditions, particularly for fast-moving liquid surfaces.

Accordingly, this study aims to investigate vapor-molecule condensation with NC gas molecules under fast-moving liquid conditions, based on the mean-field kinetic theory using the Enskog–Vlasov equation. Specifically, this condition mimics a collapsing vapor bubble containing NC gas molecules. When the vapor and NC gas flow toward the condensing liquid surface, the NC gas molecules drift to prevent vapor-molecule condensation at the liquid surface [5]. Here, we performed a simulation for this phenomenon using the Enskog–Vlasov equation to determine whether the effects of the NC gases on the evaporation and condensation coefficients differ from those of stationary liquids and whether nonequilibrium effect on condensation reduces the values of these coefficients. The results were incorporated in the KBC for the Boltzmann equation analysis.

## 2. Kinetic boundary condition, evaporation coefficient, and condensation coefficient

Fig. 1(a) presents a schematic of the collapsing vapor-gas bubble and its condensing flow in a vapor-gas mixture system. In the condensing flow, we observed the liquid phase on the left side and the vapor/gas phase on the right side. An enlarged view of the interface is presented in Fig. 1(b). A vapor molecule can condense, reflect, and evaporate during the vapor/gas phase. As shown in Fig. 1(c), based on these molecular motions, the vapor molecular mass fluxes can be defined as $J^V_{\mathrm{evap}}$, $J^V_{\mathrm{ref}}$, and $J^V_{\mathrm{cond}}$, which are the evaporating mass flux, reflecting mass flux, and condensing mass flux, respectively (see Refs. [7, 9, 10, 12–15] for pure vapor, and Refs. [18–21] for gas–mixture). The mass flux outgoing into the vapor/gas phase $J^V_{\mathrm{out}}$ and the mass flux colliding with the liquid phase $J^V_{\mathrm{coll}}$ are expressed as

$$J^V_{\mathrm{out}} = J^V_{\mathrm{evap}} + J^V_{\mathrm{ref}}, \quad J^V_{\mathrm{coll}} = J^V_{\mathrm{cond}} + J^V_{\mathrm{ref}}. \tag{1}$$

Using these molecular mass fluxes, we can define the evaporation coefficients $\alpha^V_e$ and the condensation coefficients $\alpha^V_c$ as

$$\alpha^V_e = \frac{J^V_{\mathrm{evap}}}{J^{V*}_{\mathrm{out}}} = \frac{J^V_{\mathrm{evap}}}{m^V n^{V*}\sqrt{\frac{R^V T_L}{2\pi}}}, \quad \alpha^V_c = \frac{J^V_{\mathrm{cond}}}{J^V_{\mathrm{coll}}}, \tag{2}$$

where the superscript * indicates the value at the equilibrium state, $m^V$ is the mass of the vapor molecule, $n^{V*}$ is the saturated vapor number density, $R^V = k_b/m^V$ is the gas constant of the vapor, $k_b$ is the Boltzmann constant, and $T_L$ is the liquid temperature. The value of $J^V_{\mathrm{out}}{}^*$ in the equilibrium state depends on the liquid temperature and the NC gas content at the interface [20]. The expression of $J^V_{\mathrm{out}}{}^*$ is written in Ref. [9]. The value of $J^V_{\mathrm{evap}}$ also depends on the liquid temperature, based on the concept of spontaneous evaporation [9,14,23], and the NC gas content at the interface [21]. The evaporation coefficient is defined as the extent to which molecules spontaneously evaporate from a liquid relative to the saturated (equilibrium) flux, $J_{\mathrm{out}}{}^*$ [9]. The condensation coefficient, on the other hand, refers to how many molecules condense relative to the number of molecules collidng from the gas phase to the liquid phase.

These coefficients are included in the KBC [7]:

$$f^V_{\mathrm{out}} = \frac{\alpha^V_e n^{V*} + (1-\alpha^V_c) n^V_{\mathrm{ref}}}{(2\pi R^V T_L)^{3/2}} exp\left(-\frac{\xi_x^2+\xi_y^2+\xi_z^2}{2R^V T_L}\right), (\xi_x > 0), \tag{3}$$

where $\xi_x$ is the molecular velocity normal to the interface, and $\xi_y$ and $\xi_z$ are the molecular velocities tangential to the interface. $n^V_{\mathrm{ref}}$ is the density of the diffusively reflecting molecules at the interface. We obtained $n^V_{\mathrm{ref}}$ by integrating the molecular velocity distribution function (VDF) of the molecules colliding with the interface as

$$n^V_{\mathrm{ref}} = -\sqrt{\frac{2\pi}{R^V T_L}} \int_{-\infty}^{+\infty}\int_{-\infty}^{+\infty}\int_{-\infty}^{0} \xi_x f^V_{\mathrm{coll}} \mathrm{d}\xi_x \mathrm{d}\xi_y \mathrm{d}\xi_z, \tag{4}$$

Thus, the KBC represents the VDF of the molecules outgoing from the liquid phase to the vapor/gas phase. The first term of Eq. (3) denotes the

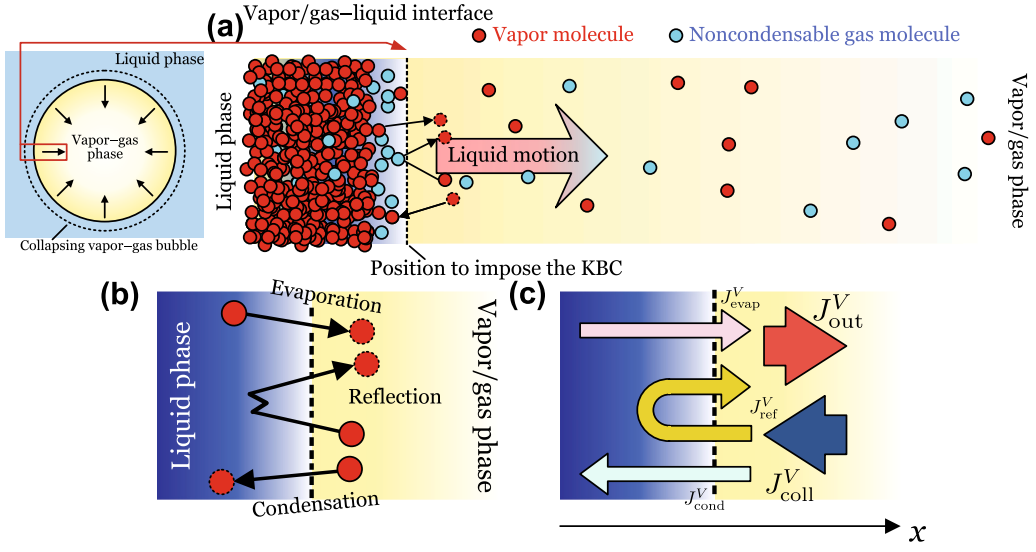


**Fig. 1.** (a) Schematic of collapsing vapor–gas bubble and moving liquid film in vapor–gas mixture system, (b) classified molecules at interface, and (c) molecular mass fluxes. At the moving-liquid surface, molecular motions can be categorized into three types: condensation, reflection, and evaporation. The corresponding molecular mass fluxes are $J^V_{\mathrm{cond}}$, $J^V_{\mathrm{ref}}$, and $J^V_{\mathrm{evap}}$, respectively. These fluxes relate $J^V_{\mathrm{coll}}$ or $J^V_{\mathrm{out}}$, as expressed in Eq. (1).

evaporation of vapor moleucles, and the second term denotes the reflection of vapor molecules at the interface. By integrating $f^V_{\rm out}$, we can derive the relation in Eq. (1): $\int_{-\infty}^{+\infty}\int_{-\infty}^{+\infty}\int_{0}^{\infty} m^V \xi_x f^V_{\rm out} d\xi_x d\xi_y d\xi_z = J^V_{\rm out} = J^V_{\rm evap} + J^V_{\rm ref}$, where $J^V_{\rm evap} = \alpha^V_e m^V n^{V*}\sqrt{R^V T_L/(2\pi)}$, and $J^V_{\rm ref} = (1-\alpha^V_c) m^V n^V_{\rm ref}\sqrt{R^V T_L/(2\pi)}$. Recent studies have shown that $\alpha^V_e$ and $\alpha^V_c$ depend on the liquid temperature and the amount of NC gas molecules accumulated at the gas-liquid interface (e.g., Refs. [20, 21]). The KBC shown in Eq. (3) is conventionally used for the weak non-equilibrium state. Additionally, the KBC for NC gas molecules, $f^G_{\rm out}$, is regarded as a diffusion reflection condition, that is, $\alpha^G_e = \alpha^G_c = O(10^{-3}) \approx 0$ [19], where $\alpha^G_e$ and $\alpha^G_c$ are similarly defined by Eq. (2) for NC gas molecules by changing the superscript $V$ to $G$; $V$ denotes vapor and $G$ denotes NC gas.

## 3. Methods

### 3.1. Enskog–Vlasov equation and numerical solver

We used the Enskog–Vlasov equation [24], which can be used to treat both the vapor/gas and liquid phases [25], to simulate a fast–moving liquid film and the surrounding mixture gas. The equation for the spatially one-dimensional form is as follows:

$$\frac{\partial f^V}{\partial t} + \xi_x \frac{\partial f^V}{\partial x} + \left(\frac{F^{VV}_x}{m^V} + \frac{F^{VG}_x}{m^V}\right)\frac{\partial f^V}{\partial \xi_x} = C_E\left(f^V, f^V\right) + C_E\left(f^V, f^G\right), \tag{5a}$$

$$\frac{\partial f^G}{\partial t} + \xi_x \frac{\partial f^G}{\partial x} + \left(\frac{F^{GG}_x}{m^G} + \frac{F^{GV}_x}{m^G}\right)\frac{\partial f^G}{\partial \xi_x} = C_E\left(f^G, f^G\right) + C_E\left(f^G, f^V\right), \tag{5b}$$

where $f^i(x,\xi,t)$ is the VDF, with the superscript $i = (V, G)$ denoting vapor ($V$) or NC gas ($G$); $t$ is the time; $x$ is the position; and $\xi = (\xi_x, \xi_y, \xi_z)$ is the molecular velocity. Further, $F^{ij}_x$ is the attractive mean-field force, with the superscript $ij = (VV, VG, GV, GG)$ representing the attraction between vapor and vapor ($VV$), vapor and NC gas ($VG$ and $GV$), or NC gas and NC gas ($GG$). $C_E$ denotes the collision term [26]. This equation assumes that the molecules interact according to the following intermolecular potential (i.e., the Sutherland potential):

$$\psi^{ij} = \begin{cases} +\infty & (r \le \sigma^{ij}) \\ -\phi^{ij}\left(\dfrac{\sigma^{ij}}{r}\right)^{\gamma} & (r > \sigma^{ij}), \end{cases} \tag{6}$$

where $\phi^{ij}$ denotes the depth of the potential well, $\sigma^{ij}$ denotes the molecular diameter, $r$ denotes the distance between two interacting molecules, and $\gamma(=6)$ denotes a parameter related to the potential. This molecular potential consists of the repulsive and attractive parts. The repulsive part is expressed by the hard sphere as the collision term ($C_E$ in Eqs. (5a) and (5b)), and the attracting part, which asymptotically behaves as with 12–6 Lennard-Jones potential, is incorporated into the mean-field term ($F^{ij}_x$ in Eqs. (5a) and (5b)). In this study, we set $\phi^{VV} = 1.325 k_b T^V_{\rm cri}$, $\phi^{VG} = \phi^{GV} = 0.364 k_b T^V_{\rm cri}$, and $\phi^{GG} = 0.1 k_b T^V_{\rm cri}$. These values are identical to those obtained in a previous study [20]. By setting these parameters in this study, simulations of the same molecular species under different nonequilibrium conditions can be investigated. Here, $T^V_{\rm cri}$ is the critical vapor temperature. In this setting, the vapor molecules can condense, whereas the NC gas molecules cannot condense. The molecular mass and diameter were the same for the vapor and the NC gas, i.e., $m = m^V = m^G$ and $\sigma = \sigma^{ij}$, respectively. These are termed as mechanically identical molecules [25,27–29] and enable us to focus on the NC gas-content effect alone. Even under these assumptions, the behavior of the vapor and NC gas in this simulation in evaporation and condensation phenomena is in qualitative agreement with the MD simulation [21]. Moreover, macroscopic quantities such as the density, velocity, and temperature can be obtained by integrating $f^i$ in the velocity space.

We used the Enskog–Vlasov direct simulation Monte Carlo (EVDSMC) method as the numerical scheme for the equation. This simulation method was proposed by Frezzotti et al. [30,31] as an extension of the standard scheme for the Boltzmann equation, that is, the direct simulation Monte Carlo (DSMC) method [32]. This EVDSMC method has been used in several studies investigating the phase transition problem [11–15,20,33]. The trends of the evaporation and condensation coefficients obtained by the EVDSMC method using the molecular potential mentioned above [12–14,19,20] have been consistent with molecular dynamics results for pure vapor [9,10,23] and vapor with NC gas cases [18,21].

### 3.2. Simulation setting

The simulation settings are described in this section. A spatially one-dimensional problem is solved using the Enskog–Vlasov equation. Fig. 2 (a) presents the schematic of the simulation settings. Although this is a one-dimensional problem and thus cannot handle the effect of interface curvature, the effect of curvature on the phase change is more pronounced at the nanosize level [7], so most of the bubble collapse phenomena can be simulated with a one-dimensional evaporation/condensation. Initially, a liquid film was adopted at the center of the system with a width of $L = 1000\sigma$; the vapor and NC gas surrounded this film. A periodic boundary condition was imposed at $x = \pm 500\sigma$, and the initial equilibrium conditions were as follows: (i) We arranged the vapor sample molecules, the number of which corresponds to the saturated-vapor number density in the system outside the region of $[-15\sigma, +15\sigma]$. We also uniformly arranged those corresponding to the equilibrium liquid density inside the region $[-15\sigma, +15\sigma]$. (ii) We uniformly arranged the NC gas sample molecules outside the region $[-15\sigma, +15\sigma]$, where the NC gas amount varied across the simulation cases. (iii) After sufficient time, by controlling the liquid temperature ($T_L = 0.60 T^V_{\rm cri}$), equilibrium states were formed as the initial state.

Once we obtained the initial equilibrium condition, we added the $x$-direction velocity $V_x(t=0)$, which is comparable with the speed of sound of the gas, to the liquid film, whose region is $[X^-_m - \delta/2, X^+_m + \delta/2]$, at non-dimensional time $\widehat{t} = t\sqrt{2RT^V_{\rm cri}}/\sigma = 0$. Here, $X^-_m$ and $X^+_m$ are the center positions of the density transition layer, and $\delta$ is its thickness (Fig. 2(b)). These values were obtained using the so-called 10–90 thickness equation [7,9] as follows:

$$n^V(x) = \frac{n^V_{\rm vap} + n^V_{\rm liq}}{2} \pm \frac{n^V_{\rm vap} - n^V_{\rm liq}}{2} tanh\left(\frac{x - X_m}{0.455\delta}\right), \tag{7}$$

where $n^V_{\rm vap}$ is the bulk vapor density, and $n^V_{\rm liq}$ is the bulk liquid density. This equation was fitted to the density field in the equilibrium state in the absence of NC gas molecules. Thus, systems of the fast–moving liquid film were realized, which resulted in non-equilibrium states. The motion of the liquid film causes net evaporation of the liquid at the interface on the left side of the film and net condensation at the interface on the right side of the film. The net evaporation behind the liquid film suppressed the increase in film temperature owing to the net condensation in front of the film. Additionally, the NC gas molecules drifted at the condensing surface. In the simulation results shown below, the compressional waves generated by the initial movement of the liquid phase do not return to the liquid film surface, so the effect of the system boundary can be neglected.

The simulation cases were realized by changing the NC gas content and the drift velocity of the liquid film, as shown in Table 1. Four independent simulations were performed, and we adopted the ensemble averages for each case. The cell size was $\Delta x = 0.2\sigma$, and the time step was $\Delta t = 0.0005\sigma/\sqrt{2RT^V_{\rm cri}}$. The number of sample molecules per cell corresponding to the critical density was set as $N_0 = 1{,}500$.

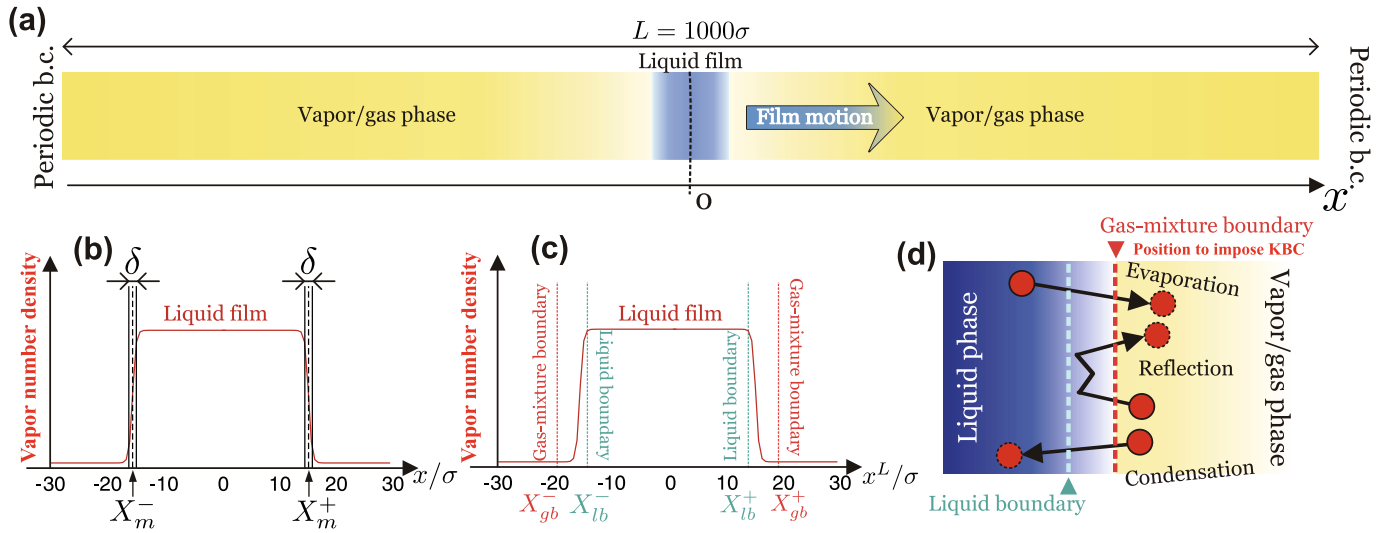


**Fig. 2.** (a) Present simulation system; (b) center position, $X_m^{\pm}$, and thickness, $\delta$, of the density transition layer; (c) liquid boundary, $X_{lb}^{\pm}$, and gas-mixture boundary, $X_{gb}^{\pm}$; and (d) categorizing molecules using the two boundaries.

**Table 1**
Simulation cases. $V_x(0)$ is the initial film velocity. $N^V$ is the total number of vapor sample molecules in the system, and $N^G$ is the total number of gas sample molecules in the system.

| Case no. | $V_x(0)/\sqrt{2RT_{\mathrm{cri}}^V}$ | $N^V$ | $N^G$ |
|---|---|---|---|
| 1 | 0.50 | 858,420 | 50,000 |
| 2 | 0.50 | 858,420 | 150,000 |
| 3 | 0.50 | 858,420 | 450,000 |
| 4 | 1.00 | 858,420 | 50,000 |
| 5 | 1.00 | 858,420 | 150,000 |
| 6 | 1.00 | 858,420 | 450,000 |
| 7 | 1.25 | 858,420 | 50,000 |
| 8 | 1.25 | 858,420 | 150,000 |
| 9 | 1.25 | 858,420 | 450,000 |

### 3.3. Classification of molecular mass fluxes

Here, we explain the method for classifying the molecular mass fluxes, which are required to evaluate the evaporation and condensation coefficients. We used two virtual boundaries, the gas-mixture boundary and liquid boundary, to determine the type of molecular mass flux at the interface. This method is referred to as the improved interphase boundary method, and it was proposed by one of the authors [18,23].

The procedure for classifying the molecules is described below. The gas-mixture boundary was imposed on the gas-mixture side, and the liquid boundary was imposed on the liquid side, as shown in Fig. 1(c), where the position of the gas-mixture boundary is that to impose the KBC. Molecules were categorized into three types: evaporating, reflecting, and condensing. Evaporating molecules were defined as the molecules crossing the gas-mixture boundary after crossing the liquid boundary; reflecting molecules were defined as the molecules crossing the gas-mixture boundary twice, without crossing the liquid boundary; and condensing molecules were defined as the molecules crossing the liquid boundary after crossing the gas-mixture boundary (Fig. 2(d)). Once the molecules were classified, the values of the molecular mass fluxes were calculated using the following equation:

$$J = \frac{mN}{S\Delta t}, \tag{8}$$

where $N$ denotes the number of molecules crossing the boundaries, $S$ denotes the cross-sectional area of the system, and $\Delta t$ denotes the sampling interval. The abovementioned classification was conducted on a coordinate system fixed at the center of the moving liquid film.

$$x^L = x - X^L, \tag{9}$$

where $X^L(t) = (X_t^- + X_t^+)/2$. $X_t^-(t)$ and $X_t^+(t)$ are the positions where the density is equal to $(n_{\mathrm{vap}}^V + n_{\mathrm{liq}}^V)/2$ for each interface. $X_t^-(t)$ and $X_t^+(t)$ are recorded in the first simulation. Subsequently, a second simulation was conducted to classify the molecules. The position of the gas mixture boundary at the condensing surface was $x^L = X_{gb}^+ = X_t^+ + 3\delta$ and that of the liquid boundary was $x^L = X_{lb}^+ = X_t^+ - \delta$, as in previous studies [18,20,23]. Here, $\delta$ is a function of the liquid temperature, and it is determined from the results of the first simulation. In addition, $x^L = X_{gb}^+$ is considered as the position to impose the KBC. We performed the simulations based on the setting and procedure described in this section.

## 4. Results and discussion

### 4.1. Macroscopic quantities

Based on the method and simulation setting described in Section 3, a program was written in C++ and calculations were performed. The CPU used in the calculations was an AMD EPYC 7713P. Fig. 3 shows a typical example of liquid film motion obtained from the simulation (Case 5). Fig. 3(a) presents the time history of the moving liquid film. Each number shown in the figure represents a non-dimensional time. As shown in the figure, the liquid film moves as time elapses, with liquid velocity $V_x(t)$. As the liquid moved, the bulk liquid density near the interface on the right-hand side decreased, indicating that the density distribution inside the liquid had a negative gradient. This is because the fast movement of the liquid causes the net condensation at the right-hand side interface, and conversely, the net evaporation of the liquid at the left-hand side interface. Due to the effects of evaporation and condensation, the temperature of the liquid near the right interface is higher, while the temperature at the left interface is lower, creating a positive temperature gradient inside the liquid. This temperature distribution also produces a non-uniform density gradient inside the liquid. Fig. 3(b) shows the velocity of the liquid film as a function of time, $V_x(t) = \mathrm{d}X^L/\mathrm{d}t$, compared with the non-dimensional speed of sound in the vapor/gas phase at $T^i = T_L = 0.60T_{\mathrm{cri}}^V$, $\sqrt{(5RT_L)/3}/\sqrt{2RT_{\mathrm{cri}}^V} = 0.707$. It is evident that the liquid velocity gradually decreases linearly over time owing to the drag force of the gas mixture; however, the liquid film moves supersonically. We confirmed that for Cases 1–3, where the initial

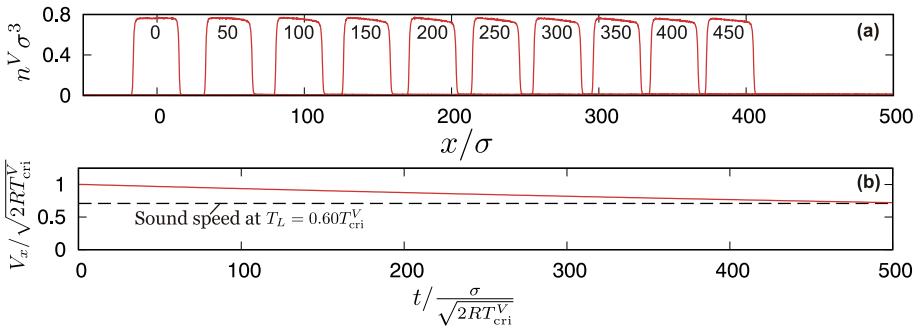


**Fig. 3.** (a) Moving liquid film from the simulation (Case 5), and (b) film velocity as a function of time. In (a), the numbers denote the non-dimensional time. In (b), the dotted line denotes the speed of sound of the gas mixture at the initial condition.

liquid film velocity is $0.5\sqrt{2RT^V_{\rm cri}}$ at dimensionless time 400, the velocity decreases by 9.28%, 14.22%, and 38.18%, respectively, relative to the initial liquid film velocity. For Cases 4–6, where the initial liquid film velocity is $1.0\sqrt{2RT^V_{\rm cri}}$, the reduction is 15.23%, 23.2%, and 42.23%, respectively, and for Cases 7–9, where the initial liquid film velocity is $1.25\sqrt{2RT^V_{\rm cri}}$, the reduction is 14.64%, 25.22%, and 53.34%, respectively.

Fig. 4 shows the macroscopic quantities of Case 5 in the coordinate system fixed at the center of the moving liquid film, $x^L$. We focused on the condensing side (interface of the liquid on the right-hand side). Figs. 4(a) and (b) show the time histories of the number density fields for the vapor and NC gas, respectively. The vapor was compressed by the film motion, and the compressed region extended toward the front over time. Additionally, we observed that the NC gas molecules drifted at the condensing surface owing to their noncondensable property. Both behaviors have been reported in previous studies that numerically simulated collapsing vapors or vapor-gas bubbles [5,34].

Figs. 4(c) and (d) show the time histories of the velocity fields normal to the interface for the vapor and the NC gas, respectively. For the early stage, the vapor and NC gas velocities toward the film can be expressed as $-V_x(0)$. These velocities then decreased with time, especially around the liquid film; this implies that the surrounding vapor and NC gas moved with the liquid film.

Figs. 4(e) and (f) show the time histories of the temperature fields for the vapor and NC gas, respectively. High temperatures, that is, near-critical temperature, were realized in front of the condensing surface owing to the gas-mixture compression. Subsequently, the high-temperature region propagated in front of the liquid film.

We consider that the flow fields observed in this simulation correspond to condensing half-space problem studied in molecular gas dynamics [6]. Next, we obtained the molecular mass fluxes at the vapor/gas interface, which, in turn, we used to determine the evaporation and condensation coefficients.

### 4.2. Molecular mass fluxes at condensing interface

The time histories of the molecular mass fluxes at the condensing interface obtained using the method described in Sec. 3.3 as well as the liquid temperature and NC gas content at the interface are shown in Fig. 5. All the displayed quantities were averaged over a duration of $5\sigma/\sqrt{2RT^V_{\rm cri}}$.

Fig. 5(a) shows the time history of the liquid temperature $T_L = T^V(x^L = X^+_{\rm lb}, t)$. This figure indicates that the temperature increases steeply at the early stage but tends to decrease slightly after reaching its peak. In this simulation, net condensation occurred on the right-hand surface; however, net evaporation occurred at the opposite interface, resulting in a slight decrease in temperature.

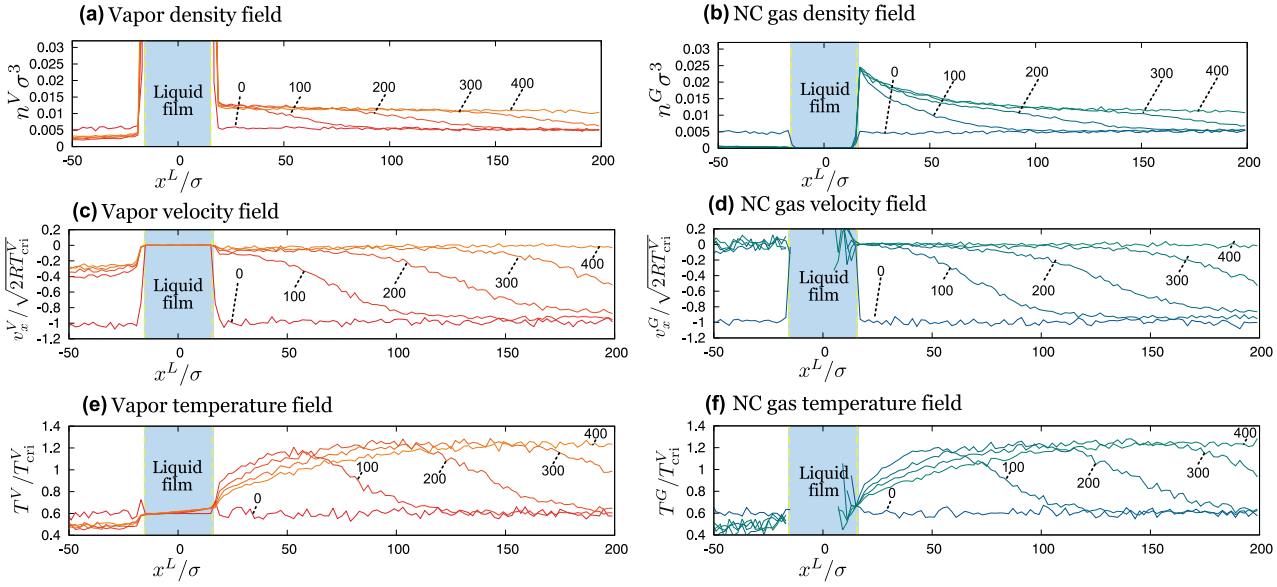


**Fig. 4.** Results of macroscopic quantities for Case 5: density fields for (a) the vapor, $n^V\sigma^3$, and (b) the NC gas, $n^G\sigma^3$; velocity fields for (c) the vapor, $v^V_x/\sqrt{2RT^V_{\rm cri}}$, and (d) the NC gas, $v^G_x/\sqrt{2RT^V_{\rm cri}}$; and temperature fields for (e) the vapor, $T^V/T^V_{\rm cri}$, and (f) the NC gas, $T^G/T^V_{\rm cri}$. The numbers denote the non-dimensional time.

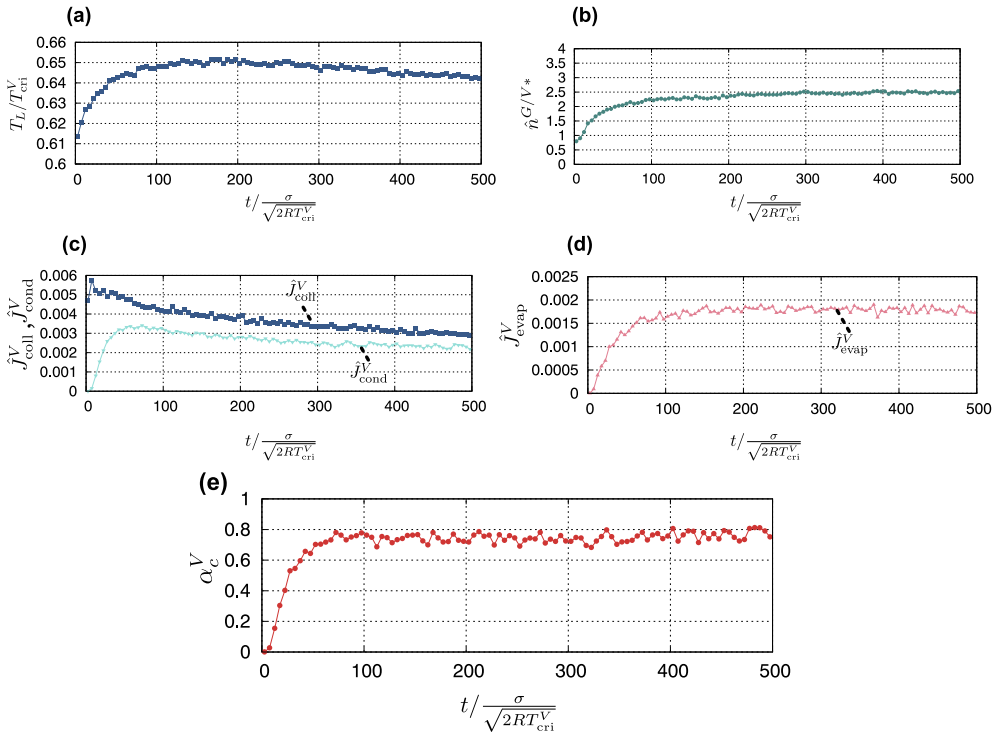


**Fig. 5.** Time history results for Case 5: (a) liquid temperature at the liquid boundary $T_L = T^V(x^L = X^+_{\rm lb}, t)$; (b) NC gas content at the gas mixture boundary $n^{G/V*}(x^L = X^+_{\rm gb}, t)$; (c) nondimensional molecular mass fluxes for condensation coefficients $\hat{J}^V_{\rm coll}$ and $\hat{J}^V_{\rm cond}$; (d) nondimensional molecular mass fluxes for the evaporation coefficients $\hat{J}^V_{\rm evap}$; and (e) the condensation coefficient using the mass fluxes shown in Fig. 5(c).

Fig. 5(b) shows the time history of the NC gas content at the gas mixture boundary of the condensing surface.

$$\hat{n}^{G/V*} = n^G\left(x^L = X^+_{\rm gb}, t\right)\Big/ n^{V*}_p, \tag{10}$$

where $n^{V*}_p$ denotes the saturated-vapor number density in the absence of NC gas molecules [20]. The figure indicates that the density ratio is almost constant after $\hat{t} = 100$. This, in turn, suggests that an almost constant amount of NC gas was accumulated at the interface.

Figs. 5(c) and (d) show the time histories of the nondimensional molecular mass fluxes at the interface. These fluxes were sampled with the time window $1\sigma/\sqrt{2RT^V_{\rm cri}}$ (summation value of 2,000 iterations). Fluxes $\hat{J}^V_{\rm coll}$ and $\hat{J}^V_{\rm cond}$ are shown in Fig. 5(c), and $\hat{J}^V_{\rm evap}$ is shown in Fig. 5(d). The illustrations indicate that the mass fluxes are almost constant, although they decrease slightly after $\hat{t} = 100$ in the dimensionless time. These fluxes start from zero at the initial stage of the simulation because the molecules between the liquid and gas boundaries cannot be divided into evaporating, condensing, and reflecting molecules by definition. However, as we confirmed that no such molecules exist after $\hat{t} = 100$, we used the fluxes after 100 in the dimensionless time below.

The coefficient is obtained using the fluxes after $\hat{t} = 100$. However, because of the unsteady nonequilibrium nature of the flow, it is difficult to accurately estimate the value of $J^V_{\rm out}{}^*$ at the equilibrium state as the function of the liquid temperature and the NC gas content, which is required to determine the evaporation coefficient. Hence, we present the condensation coefficient in the next section, and discuss the coefficients accordingly.

Figs. 5(e) shows the results of obtaining the condensation coefficient using the mass fluxes shown in Fig. 5(c). From this figure, it can be seen that each mass flux changes with time, but the value of the condensation coefficient remains constant. Previous studies [20,21] have shown that the value of condensation coefficient is affected by the temperature of the liquid and the amount of NC gas at the interface, which may be due to the fact that these values are nearly constant, as shown in Figs. 5(a) and (b).

### 4.3. Condensation coefficients

The condensation coefficient was obtained using Eq.(2). We averaged the fluxes at intervals when the liquid temperature was almost constant. For example, in Case 5, almost all the values during $100 \le \hat{t} \le 200$ can be considered constant (see Fig. 5). The condensation coefficients were then calculated. The sampling interval and results in Table 2 are presented in Fig. 6. In the table, the bar denotes the time-averaged values.

Fig. 6 presents the condensation coefficient as a function of the NC gas content, $\hat{n}^{G/V*}$, and liquid temperature, $T_L/T^V_{\rm cri}$. The red surface represents the values of the evaporation and condensation coefficients obtained in our previous studies using the following equations:

$$\begin{aligned}\alpha^V = A\left(^{T_L} + B\left(T_L/T^V_{\rm cri}\right)\hat{n}^{G/V*}\right.\\ \left.+C\left(T_L/T^V_{\rm cri}\right) + D\hat{n}^{G/V*} + E,\right.\end{aligned} \tag{11}$$

**Table 2**
Simulation results of the time-averaged condensation coefficient, compared with values obtained under equilibrium states.

| Case no. | Sampling interval | $\overline{\hat{n}}^{G/V*}$ | $\overline{T}_L/T^V_{\rm cri}$ | $\overline{\alpha}^V_c$ | $\alpha^V$ |
|---|---|---|---|---|---|
| 1 | $200 \le \hat{t} \le 400$ | 0.665 | 0.621 | 0.834 | 0.855 |
| 2 | $200 \le \hat{t} \le 200$ | 1.896 | 0.617 | 0.817 | 0.831 |
| 3 | $100 \le \hat{t} \le 200$ | 4.981 | 0.618 | 0.759 | 0.756 |
| 4 | $100 \le \hat{t} \le 200$ | 0.825 | 0.653 | 0.768 | 0.801 |
| 5 | $100 \le \hat{t} \le 200$ | 2.289 | 0.650 | 0.739 | 0.757 |
| 6 | $100 \le \hat{t} \le 200$ | 5.718 | 0.648 | 0.674 | 0.646 |
| 7 | $100 \le \hat{t} \le 200$ | 0.858 | 0.675 | 0.707 | 0.760 |
| 8 | $100 \le \hat{t} \le 200$ | 2.328 | 0.670 | 0.672 | 0.710 |
| 9 | $100 \le \hat{t} \le 150$ | 5.522 | 0.669 | 0.577 | 0.587 |

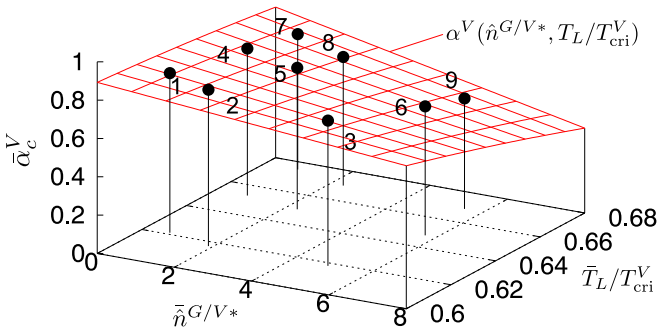


**Fig. 6.** Time-averaged condensation coefficients obtained from simulation results, and equilibrium value surface $\alpha^V(n^{G/V*}, T_L/T^V_{\rm cri})$ obtained from the previous study. The number near each result represents the case number. These values are shown in Table 2.

where $A = -5.438$, $B = -0.306$, $C = 5.623$, $D = 0.165$, and $E = -0.523$. Our previous studies showed that the evaporation and condensation coefficients under equilibrium and weak nonequilibrium states are equal [19,20]; thus, they are represented by $\alpha^V$ alone, where $\alpha^V = \alpha^V_e = \alpha^V_c$.

As shown in Fig. 6, the trend of the coefficient depends on the NC gas content, $\bar{\hat{n}}^{G/V^*}$, and the liquid temperature, $\bar{T}_L/T^V_{\rm cri}$. The coefficient decreases with an increase in $\bar{\hat{n}}^{G/V^*}$ and $\bar{T}_L/T^V_{\rm cri}$. This implies the equilibrium state values represent the coefficient well, even in such a nonequilibrium state of the fast-moving liquid system, in addition to the steady nonequilibrium problem [20]. The next section describes the verification of $\alpha^V(\bar{\hat{n}}^{G/V^*}, T_L/T^V_{\rm cri})$ based on Boltzmann equation analyses. This comparison enabled us to check whether the value of the evaporation coefficient, which could not be determined in our simulation, was equal to the value of the condensation coefficient obtained in previous studies.

Furthermore, it is important to emphasize that the condensation coefficient does not take the value $O(10^{-2})$. This indicates that, in the velocity range of the present liquid, there is no evidence of nonequilibrium effect on condensation.

## 5. Boltzmann equation analysis

We conducted an unsteady Boltzmann equation analysis using the KBC, as shown in Eq. (3), where $\alpha^V_e = \alpha^V_c = \alpha^V(\bar{\hat{n}}^{G/V^*}, T_L/T^V_{\rm cri})$, (Eq. (11)). For the analysis of the Boltzmann equation, KBCs were imposed at $x^L = X^+_{\rm gb}$. The initial condition was specified as the equilibrium at $T^i = 0.60T^V_{\rm cri}$ with an $x$-direction velocity, $-0.938\sqrt{2RT^V_{\rm cri}}$, uniformly. This initial velocity was determined as the average value of $V_x$ before $\hat{t} = 200$, because we were concerned with this time interval, and the film velocity was constant up to this time. Far from the interface ($x^L = X^+_{\rm gb} + 1000\sigma$), the molecular velocity distribution function is the Maxwellian with the saturated vapor density and $x$-direction velocity. For the NC gas molecules, the boundary condition of the diffusion reflection is imposed at the vapor–liquid interface, and the initial condition is imposed with the $x$-direction velocity. The boundary condition at infinity is given by the same velocity distribution function as that for the initial condition.

To solve the Boltzmann equation, we used the DSMC method. The cell size was $\Delta x = 4\sigma$, and the time step was $\Delta t = 0.001\sigma/\sqrt{2RT^V_{\rm cri}}$. Case 5 was selected as the simulation to be performed. Throughout the simulation, the liquid temperature for Eq. (3) remained fixed at $T_L = 0.65T^V_{\rm cri}$.

Fig. 7 shows the DSMC results, as compared with those of the EVDSMC simulation. The output of the DSMC simulation was averaged for the two cells. Notably, the time histories of the macroscopic

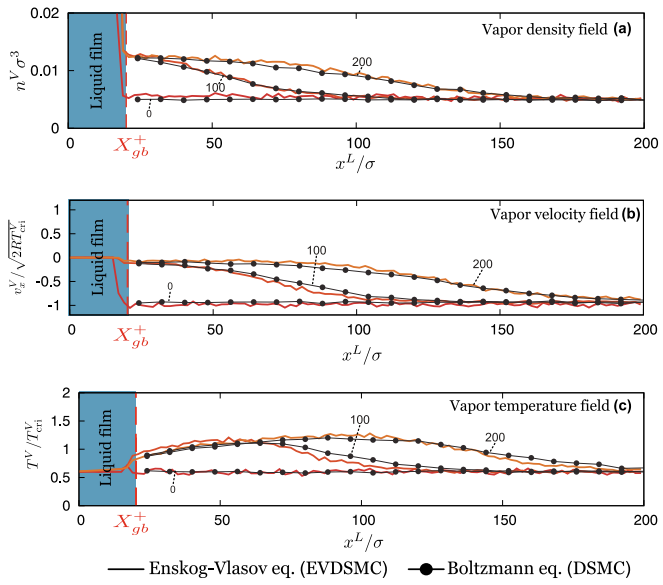


**Fig. 7.** Comparison of time history results between the Enskog–Vlasov and Boltzmann equations for (a) vapor density fields, (b) vapor velocity fields, and (c) vapor temperature fields, considering Case 5. The numbers denote the nondimensional time.

quantities reproduced the EVDSMC results well. These results indicate that the evaporation and condensation coefficients have the same value and that the value obtained in equilibrium (Eq. (11)) can be used even though we were unable to obtain the value of the evaporation coefficient from our EVDSMC results.

Based on these results, we can conclude that the evaporation and condensation coefficients in equilibrium states can be used for nonequilibrium states, such as those of fast-moving liquid systems. If the liquid temperature field is solved with the macroscopic equation (e.g., the advection–diffusion equation), we can analyze both the liquid and vapor/gas phases, without simultaneously performing molecular simulations. This is advantageous in terms of computing costs. Furthermore, these KBCs can be used to derive fluid dynamics boundary conditions that correctly describe heat and mass transport at the interface.

## 6. Conclusion

The vapor condensation phenomena with fast-moving liquid films were simulated to clarify the interfacial transport of macroscopic quantities containing NC gas molecules. In particular, the evaporation and condensation coefficients incorporated into the KBC were investigated. The simulation results showed that the condensation coefficient decreased with an increase in the NC gas content at the interface and the liquid temperature. In addition, we found that the evaporation and condensation coefficients followed the values obtained under the equilibrium state. This finding was verified via a Boltzmann equation analysis, using these coefficient values for the equilibrium state. This result was the same as that of our previous study on steady nonequilibrium states using a two-surface problem [20]. Both the current and previous studies imply that the coefficients decrease with the number of NC gas molecules at the interface. The finding aids the fluid dynamics in describing the interfacial transport of macroscopic quantities.

Furthermore, the current simulation results show that nonequilibrium effect on condensation does not occur at the liquid velocity used in this study. This effect means that vapor molecules cannot condense due to the high-speed liquid film motion, which leads to the values of condensation and evaporation coefficients are close to zero. Hence, we conclude that the condensing vapor molecules during bubble collapse decrease depending on the NC gas content at the interface. At extremely

high NC gas content conditions [19], we expect that almost no vapor molecules would condense, which, in turn, would facilitate bubble rebound.

The current study is limited to the situation interacting by mechanically identical molecules. Studies using the more realistic molecular potential (e.g., different molecular diameters/masses and polyatomic molecules such as the water–air system) will be conducted in the future.

## CRediT authorship contribution statement

**Kotaro Ohashi:** Conceptualization, Data curation, Formal analysis, Investigation, Methodology, Software, Validation, Visualization, Writing – original draft, Writing – review & editing. **Kazumichi Kobayashi:** Conceptualization, Funding acquisition, Investigation, Methodology, Project administration, Resources, Software, Supervision, Validation, Writing – review & editing. **Hiroyuki Fujii:** Supervision, Writing – review & editing. **Masao Watanabe:** Supervision, Writing – review & editing.

## Declaration of Competing Interest

The authors declare that they have no known competing financial interests or personal relationships that could have appeared to influence the work reported in this paper.

## Data availability

Data will be made available on request.

## Acknowledgments

This study was supported by JST, PRESTO Grant Number JPMJPR21O3, Japan to K.K., and JSPS KAKENHI Grant Number 20K04277 to K.K.

## References

[1] S. Fujikawa, T. Akamatsu, Effects of the non-equilibrium condensation of vapour on the pressure wave produced by the collapse of a bubble in a liquid, J. Fluid Mech. 97 (1980) 481–512.
[2] I. Akhatov, O. Lindau, A. Topolnikov, R. Mettin, N. Vakhitova, W. Lauterborn, Collapse and rebound of a laser-induced cavitation bubble, Phys. Fluids 13 (2001) 2805–2819.
[3] G.L. Chahine, A. Kapahi, C.-T. Hsiao, J.-K. Choi, Coupling bubble and material dynamics to model cavitation peening and pitting, J. Fluid Sci. Technol. 11 (2016). JFST0023–JFST0023.
[4] A. Prosperetti, Vapor bubbles, Annu. Rev. Fluid Mech. 49 (2017) 221–248.
[5] K. Kobayashi, T. Nagayama, M. Watanabe, H. Fujii, M. Kon, Molecular gas dynamics analysis on condensation coefficient of vapour during gas–vapour bubble collapse, J. Fluid Mech. 856 (2018) 1045–1063.
[6] Y. Sone (Ed.), Flows with Evaporation and Condensation, Molecular Gas Dynamics, Modeling and Simulation in Science. Engineering and Technology, Birkhäuser, Boston (2007).
[7] S. Fujikawa, T. Yano, M. Watanabe, Vapor-Liquid Interfaces, Bubbles and Droplets: Fundamentals and Applications, Springer Science & Business Media, 2011.
[8] R. Meland, A. Frezzotti, T. Ytrehus, B. Hafskjold, Nonequilibrium molecular-dynamics simulation of net evaporation and net condensation, and evaluation of the gas-kinetic boundary condition at the interphase, Phys. Fluids 16 (2004) 223–243.
[9] T. Ishiyama, T. Yano, S. Fujikawa, Molecular dynamics study of kinetic boundary condition at an interface between argon vapor and its condensed phase, Phys. Fluids 16 (2004) 2899–2906.
[10] T. Ishiyama, T. Yano, S. Fujikawa, Kinetic boundary condition at a vapor-liquid interface, Phys. Rev. Lett. 95 (2005), 084504.
[11] A. Frezzotti, L. Gibelli, S. Lorenzani, Mean field kinetic theory description of evaporation of a fluid into vacuum, Phys. Fluids 17 (2005), 012102.
[12] K. Kobayashi, K. Ohashi, M. Watanabe, Numerical analysis of vapor-liquid two-phase system based on the Enskog-Vlasov equation, AIP Conf. Proc. 1501 (2012) 1145–1151.
[13] M. Kon, K. Kobayashi, M. Watanabe, Method of determining kinetic boundary conditions in net evaporation/condensation, Phys. Fluids 26 (2014), 072003.
[14] M. Kon, K. Kobayashi, M. Watanabe, Liquid temperature dependence of kinetic boundary condition at vapor-liquid interface, Int. J. Heat Mass Transf. 99 (2016) 317–326.
[15] M. Kon, K. Kobayashi, M. Watanabe, Kinetic boundary condition in vapor-liquid two-phase system during unsteady net evaporation/condensation, Eur. J. Mech. - B/Fluids 64 (2017) 81–92.
[16] V.V. Zhakhovsky, A.P. Kryukov, V.Y. Levashov, I.N. Shishkova, S.I. Anisimov, Mass and heat transfer between evaporation and condensation surfaces: atomistic simulation and solution of Boltzmann kinetic equation, Proc. Natl. Acad. Sci. 116 (2019) 18209–18217.
[17] J. Nie, A. Chandra, Z. Liang, P. Keblinski, Mass accommodation at a high-velocity water liquid-vapor interface, J. Chem. Phys. 150 (2019), 154705.
[18] K. Kobayashi, K. Sasaki, M. Kon, H. Fujii, M. Watanabe, Kinetic boundary conditions for vapor–gas binary mixture, Microfluid. Nanofluid. 21 (2017) 53.
[19] K. Ohashi, K. Kobayashi, H. Fujii, M. Watanabe, Evaporation coefficient and condensation coefficient of vapor under high gas pressure conditions, Sci. Rep. 10 (2020) 8143.
[20] K. Ohashi, K. Kobayashi, H. Fujii, M. Watanabe, Mean-field kinetic theory analysis of vapor flow between evaporating and condensing interfaces in the presence of non-condensable gas molecules, Phys. Fluids 33 (2021), 122017.
[21] H. Tabe, K. Kobayashi, H. Fujii, M. Watanabe, Molecular dynamics simulation of evaporation coefficient of vapor molecules during steady net evaporation in binary mixture system, Int. J. Heat Mass Transf. 188 (2022), 122663.
[22] B. Murray, M.J. Fox, S. Narayan, Analyzing interfacial transport for water evaporating into dry nitrogen, Appl. Therm. Eng. 202 (2022), 117910.
[23] K. Kobayashi, K. Hori, M. Kon, K. Sasaki, M. Watanabe, Molecular dynamics study on evaporation and reflection of monatomic molecules to construct kinetic boundary condition in vapor-liquid equilibria, Heat Mass Transf. 52 (2016) 1851–1859.
[24] J. Karkheck, G. Stell, Mean field kinetic theories, J. Chem. Phys. 75 (1981) 1475.
[25] A. Frezzotti, L. Gibelli, D.A. Lockerby, J.E. Sprittles, Mean-field kinetic theory approach to evaporation of a binary liquid into vacuum, Phys. Rev. Fluids 3 (2018), 054001.
[26] P. Resibois, M. De Leener, Classical Kinetic Theory of Fluids, Wiley, 1977.
[27] Y. Sone, K. Aoki, T. Doi, Kinetic theory analysis of gas flows condensing on a plane condensed phase: case of a mixture of a vapor and a noncondensable gas, Transp. Theor. Stat. Phys. 21 (1992) 297–328.
[28] K. Aoki, S. Takata, S. Kosuge, Vapor flows caused by evaporation and condensation on two parallel plane surfaces: effect of the presence of a noncondensable gas, Phys. Fluids 10 (1998) 1519–1533.
[29] S. Taguchi, K. Aoki, S. Takata, Vapor flows condensing at incidence onto a plane condensed phase in the presence of a noncondensable gas. I. Subsonic condensation, Phys. Fluids 15 (2003) 689–705.
[30] A. Frezzotti, A particle scheme for the numerical solution of the Enskog equation, Phys. Fluids 9 (1997) 1329–1335.
[31] A. Frezzotti, P. Barbante, L. Gibelli, Direct simulation Monte Carlo applications to liquid-vapor flows, Phys. Fluids 31 (2019), 062103.
[32] G.A. Bird, Molecular Gas Dynamics and the Direct Simulation of Gas Flows, Clarendon press Oxford, 1994.
[33] S. Busuioc, L. Gibelli, D.A. Lockerby, J.E. Sprittles, Velocity distribution function of spontaneously evaporating atoms, Phys. Rev. Fluids 5 (2020), 103401.
[34] Y. Hao, Y. Zhang, A. Prosperetti, Mechanics of gas-vapor bubbles, Phys. Rev. Fluids 2 (2017), 034303.